Historical & future maximum ocean temperatures

B. B. Cael[1], Friedrich A. Burger[2,3], Stephanie A. Henson[1], Gregory L. Britten[4], Thomas L. Frölicher

1. National Oceanography Centre, Southampton, UK. 2. Climate and Environmental Physics, Physics Institute, University of Bern, Switzerland. 3. Oeschger Centre for Climate Change Research, University of Bern, Switzerland. 4. Woods Hole Oceanographic Institution, Woods Hole, MA, USA.

*cael@noc.ac.uk.

This is a non-peer reviewed preprint submitted to EarthArXiv.

Significance Statement: Marine heatwaves have become common, and are expected to become more frequent and intense going forwards. While the models used to estimate the risks of future marine heatwaves can reproduce the specifics of some individual extreme events, it is not known whether they capture the statistical properties of extreme ocean temperatures on the whole, and therefore how reliable their projections of marine heatwaves in the future really are. We show that observations of maximum ocean surface temperatures conform well to expectations from extreme value theory. Via this theory, we show that Earth system models capture the statistical properties of ocean's maximum temperatures. We can thus leverage these models to project how maximum ocean temperatures will evolve under continued global warming.

Abstract: Marine heatwaves impact ocean ecosystems and are expected to become more frequent and intense with continued global warming. The ability of Earth system models to reproduce the statistical characteristics of extreme ocean temperatures has not yet been tested quantitatively, making the reliability of their future projections of marine heatwaves uncertain. We demonstrate that annual maxima of detrended anomalies in daily-mean sea surface temperatures over the last 39 years of global satellite observations are described excellently by the Generalised Extreme Value (GEV) distribution, as predicted from extreme value theory. GEV parameters' spatial patterns conform to physical expectations, further supporting its use for model-observation comparison. Historical realisations of 14 CMIP6 Earth system models reproduce the GEV and spatial patterns in the underlying parameters. We can

then use these models with confidence to project future changes in maximum ocean temperatures, which we show will become warmer (by 1.08±0.18°C on average under 2° warming and 2.06±0.19°C on average under 3.2°C warming) and tend to increase more than global mean sea surface temperature (0.92±0.18°C and 1.77±0.14°C respectively). Our study provides an effective means to quantify extreme ocean temperatures, as well as confidence in the predictions of future marine heatwaves from CMIP6 models.

Marine heatwaves (MHWs) - anomalously high ocean temperatures [20] - can extend thousands of kilometers and last for weeks to years [21, 24]. MHWs have occurred in all ocean basins over the last few decades [13, 31] and often caused devastating impacts on marine ecosystems [34], ranging from habitat shifts [6] and changes in population structure [4] to high mortality of various marine keystone species [23, 33]. These extreme events can overwhelm the capacity of both natural and human systems to cope, potentially causing socioeconomic impacts such as loss of essential ecosystem services and fisheries income [34, 5]. The frequency of MHWs has increased over the last century [30], including a doubling over the satellite period [13], mainly due to anthropogenic climate change [13, 24]. The frequency and intensity of MHWs are projected to increase in the future as global temperatures are projected to continue to rise [13, 31] with potentially widespread consequences for marine ecosystems globally.

The generalized extreme value (GEV) distribution is a popular and well-established statistical model to describe the maxima of temperature distributions (or maxima of any other time series data) [7]. The GEV distribution has been applied to study, for example, extreme temperatures and precipitation on land [22, 29, 16, 35, 11]. While there has been some application of the GEV in marine contexts [2, 25], it remains underutilised in oceanic applications and in particular in studies of marine heatwaves.

Analogous to the Gaussian distribution and the central limit theorem [3], many natural phenomena's maxima are GEV-distributed, explained by the extreme value theorem [7]. The GEV distribution's three parameters, location (μ), scale (σ), and shape (ξ), respectively, roughly determine its central value, its variability, and the weight of its upper tail (Methods). The advantage of a distributional approach is that if the GEV can describe the variability in observation-based sea surface temperature (SST, °C) maxima, this simplifies the description and quantitative comparison with climate models. The question becomes how GEV-like modeled and observed SST maxima are, what the parameters of the associated distributions are, and how these parameters vary in space and under global warming when estimated for individual locations.

Our analysis starts with the hypothesis that SST maxima are GEV-distributed. Here we confirm this hypothesis for satellite-derived annual maxima of mean daily SST, then use it to demonstrate that simulated SST by the latest generation of Earth system models that participated in Phase 6 of the Coupled Model Intercomparison Project (CMIP6; [10]) capture the statistical characteristics of surface ocean temperature extremes well, and utilise this to make inferences about future ocean temperature extremes under two different global warming scenarios.

Results

The generalized extreme value distribution (GEV) is appropriate for modeling annual maxima in sea surface temperature (Figure 1). When pooling all annual maxima of linearly detrended SST anomalies over the 39-year 1982-2020 observation period over all grid cells across the globe (see Methods), the GEV distribution captures the shape of the empirical distribution excellently. The global GEV distribution is approximately a Gumbel distribution, since the shape parameter is close to zero ($\xi = -0.01$). No significant trends in the parameter estimates can be found over the 39-year period, as the parameter estimates of distributions for individual years do not change systematically with time, indicating that the distribution of the annual maxima of detrended SST anomalies is stationary (Methods).

At the local scale, the GEV is fitted to detrended SST anomalies as well as to raw SST data (see Methods). The goodness of fit is assessed based on the median Kuiper statistic, which quantifies the difference between two distributions in terms of the maximum differences in their cumulative distribution functions (Methods), across all grid cells. The Kuiper statistic is similar to the more common Kolmogorov-Smirnov statistic but is preferred because it gives equal weight to all portions of the distribution [12]. We find a median Kuiper statistic of 0.14 (anomalies) and 0.13 (raw data). In the ideal case of sampling 39 values from a GEV distribution many times, one also obtains a very similar Kuiper statistic of 0.14, suggesting that the GEV is a good model also at the local scale. In other words, a Kuiper statistic value of 0.14 is expected for true GEV data given the sample size, which matches the values found for the observations. Similar to the global scale, the shape parameter is close to zero in most of the ocean (Figure 2c,f) and slightly negative elsewhere. The spatial pattern in the location parameter for the raw data (Figure 2d) mainly reflects the latitudinal gradients in

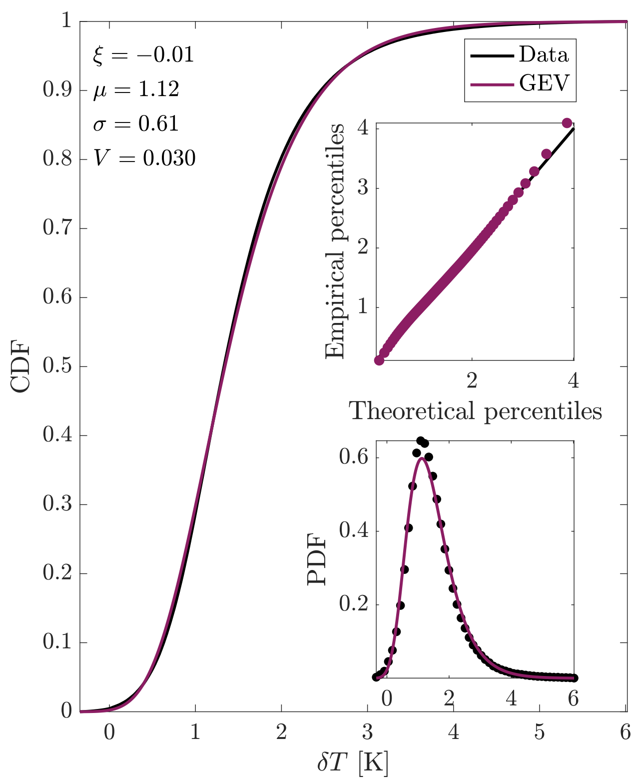

Figure 1: **Generalized extreme value (GEV) distribution fit for globally pooled maximum annual sea surface temperature anomalies.** Shown are the theoretical (fitted GEV) and empirical cumulative distribution functions (CDFs), with the corresponding probability density functions (PDFs) in the lower inset, and in the upper inset the empirical vs. theoretical percentiles overlaid on a 1:1 line. The fit parameters for shape (ξ), location (μ), and scale (σ) and the Kuiper statistic (V) are given. Data are analyzed at 1° resolution to facilitate comparison with models.

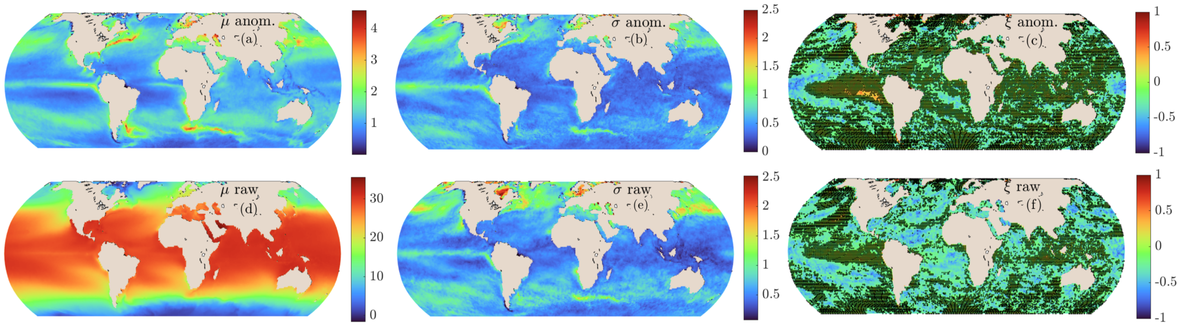

Figure 2: **Local GEV parameter estimates for the satellite SST observations.** Estimated parameters are shown for the anomalies (first row) and raw data (second row). Black stippling in (c) and (f) indicates regions where the estimate's 90 % confidence interval includes 0; no such region exists for (a), (b), (d), or (e).

sea surface temperatures, with higher maxima in low-latitude regions where SST is generally higher. For the detrended anomalies data (Figure 2a), we find the largest location parameters where SST variability is largest, such as in Western Boundary Current regions [18] and the high latitudes [9]. The scale parameter is generally large where strong interannual variability in SST drives large year-to-year variations in SST maxima (Figure 2b,e), such as in the equatorial Pacific and in the northern high latitudes. The scale parameter estimates are often larger for the raw data (median ratio σ anom./σ raw $= 0.79$, 90% range 0.56–1.16), because detrending and removing a seasonal cycle reduce the year-to-year variability in the SST maxima relative to the raw SST data (see Methods for uncertainties).

There are no systematic deviations between the CMIP6 Earth system model ensemble and the satellite observations (Table 1). For the globally pooled data, the goodness of fit matches that of the satellite observations well (model mean Kuiper statistic of 0.032 compared to 0.030 for the satellite data; Table 1). The model-mean parameter estimates are close to the estimates of the satellite product. The observations easily fall within the 90% confidence interval of the model ensemble for every parameter. The satellite-data parameter estimates are thus not significantly different from the respective model distributions. Put differently, the satellite data is indistinguishable from being another model in the CMIP6 model ensemble.

At the local scale, the models show a very similar goodness of fit as the satellite observations (median Kuiper statistic in Table 1). Furthermore, the parameter estimates agree well with those of the satellite data. The r^2 values for μ and σ that express the proportions of variance in the model estimates that can be explained by the satellite estimates are often close to 0.9 or higher (Table 1; Methods). The best match is found for the raw μ estimates, because the models and satellite observations generally

	global				anomalies			raw		
	V	μ	σ	ξ	$\tilde{V}$	$r^2(\mu)$	$r^2(\sigma)$	$\tilde{V}$	$r^2(\mu)$	$r^2(\sigma)$
Observations	**0.030**	**1.12**	**0.62**	**−0.01**	**0.14**	∼	∼	**0.13**	∼	∼
ACCESS-CM2	0.020	0.83	0.54	−0.03	0.14	0.87	0.87	0.14	0.99	0.90
ACCESS-ESM1-5	0.030	0.72	0.51	−0.01	0.14	0.83	0.87	0.14	0.99	0.89
BCC-CSM2-MR	0.036	0.77	0.49	−0.04	0.14	0.84	0.87	0.14	0.99	0.92
CanESM5	0.022	0.89	0.56	−0.01	0.14	0.82	0.77	0.15	0.99	0.75
CMCC-ESM2	0.038	1.02	0.74	−0.06	0.14	0.91	0.81	0.14	0.99	0.87
CNRM-CM6-1	0.023	1.37	0.62	+0.03	0.14	0.88	0.86	0.14	0.97	0.89
CNRM-ESM2-1	0.029	1.34	0.65	+0.05	0.14	0.81	0.81	0.14	0.98	0.86
CESM2	0.043	0.76	0.56	−0.08	0.14	0.88	0.88	0.14	0.99	0.87
GFDL-ESM4	0.018	1.30	0.64	−0.08	0.14	0.92	0.90	0.14	0.98	0.91
MIROC6	0.030	0.75	0.58	−0.04	0.13	0.82	0.85	0.14	0.96	0.89
MPI-ESM1-2-HR	0.037	0.90	0.55	−0.06	0.14	0.90	0.89	0.14	0.97	0.91
MPI-ESM1-2-LR	0.043	0.85	0.53	−0.07	0.14	0.87	0.90	0.14	0.99	0.91
NorESM2-LM	0.034	1.06	0.66	−0.06	0.14	0.91	0.86	0.14	0.98	0.83
NorESM2-MM	0.056	0.95	0.76	−0.09	0.14	0.91	0.77	0.14	0.98	0.83
Model mean	**0.032**	**0.97**	**0.60**	**−0.04**	**0.14**	**0.87**	**0.85**	**0.14**	**0.98**	**0.87**
Model 90% CI	**±0.018**	**±0.36**	**±0.13**	**±0.07**	**±0.00**	**±0.06**	**±0.07**	**±0.00**	**±0.02**	**±0.07**

Table 1: **Generalized extreme value distribution (GEV) fits for the satellite observations and CMIP6 models.** For the globally pooled anomalies, the Kuiper statistic (V) as well as the parameter estimates are shown. For the fits at each location using anomalies and raw data, the median Kuiper statistic as well as r^2 values for the simulated μ and σ parameters are shown, indicating how well the simulated parameter estimates agree with those from the observations (see Methods section). An r^2 value of 1 indicates an everywhere perfect match between the parameter estimates in a simulation and those from observations.

agree on the latitudinal temperature gradient that imprints on μ for the raw data.

Where satellite observations fall within the spread of model results in the historical period (all ocean area outside the pink stippled areas in Figure 3), one may also expect that the spread of projected changes in GEV parameters with global warming contains the 'true' change in parameters under a forcing scenario. We here focus on the location parameter for the raw data, μ_{raw}. For the other cases (σ_{raw}, ξ_{raw}, $\mu_{anom.}$, $\sigma_{anom.}$, and $\xi_{anom.}$), the models generally do not predict substantial changes nor agree on the sign of change, i.e. the 90% confidence intervals there include zero over almost all of the ocean, or the change is due to aggregating SSTs over a period with a warming trend artificially increasing the interannual variability [36] in the case of σ_{raw} (see Materials and Methods). The location parameter for the raw SST data increases almost everywhere between the observation period 1982-2020 and 2061-2100, both under SSP1-2.6 and SSP5-8.5 (Figure 3a,b). This increase is due to the mean sea surface warming that is simulated by all models in most regions. Exceptions are parts of the Southern Ocean and the North Atlantic where trends in SST are not always positive [14, 17, 26] (black stippled regions in Figure 3). Increases in the location parameter are generally larger under SSP5-8.5 than

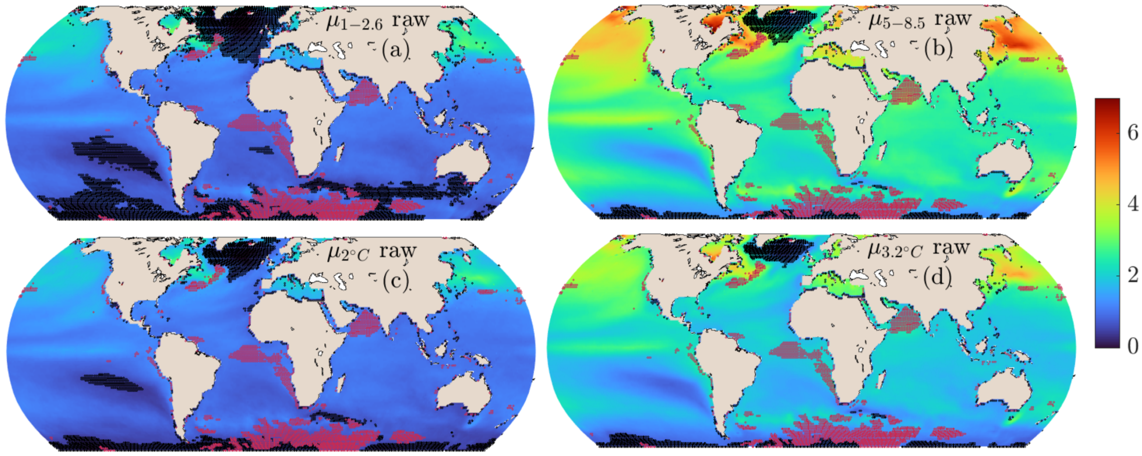

Figure 3: **CMIP6 ensemble mean change in the μ parameter between the satellite period and 2061-2100 under the SSP1-2.6 and SSP5-8.5 scenarios and 2°C and 3.2°C warming levels.** Black stippling indicates regions where the 90 % confidence interval of the model ensemble distribution includes 0, i.e., that a parameter change of 0 can not be rejected based on the model ensemble distribution. Pink stippling indicates regions where the parameter estimate from satellite observations is not contained in the 90 % confidence interval of the model ensemble distribution during the historical period. In these regions, the observed GEV distribution thus significantly differs from the models and it cannot be expected that the future parameter change can be represented by the model ensemble distribution.

under SSP1-2.6, reflecting the larger warming under SSP5-8.5 (Figure 3). Across all models and over the total ocean, the average difference in μ under SSP5-8.5 versus SSP1-2.6 in 2061-2100 is 1.24°C. Robust increases in the scale parameter are simulated for the raw data in the tropical Atlantic and Indian Ocean under the SSP5-8.5 scenario (but not SSP1-2.6); these appear to be due to increases in the warming trend rather than interannual variability changes (Materials and Methods) [36], so we do not focus on them here.

When using fixed warming levels of 2 °C and 3.2 °C instead of a fixed future period, regions where the model ensemble distribution includes zero are similar (black stippling areas in Figure 3; 3.2 °C is used as it is the maximum warming level possible to analyze given the warming in the model realizations investigated here). Thus, the disagreement between models in these regions is not primarily caused by differing warming rates between the models. Interestingly, the global average increase in the GEV-based expected value of SST maxima is 1.08±0.18°C (mean and standard deviation across models) under 2°C warming, and 2.06±0.19°C under 3.2°C warming. These changes are almost entirely (>95%) due to changes in μ, noting that all three parameters can impact the expected value of the GEV. This is slightly greater than the global mean SST increase in these models, which increase by 0.92±0.18°C and 1.77±0.14°C on average respectively, consistent with previous work [13]. This is likely because of increasing seasonal cycle amplitudes [1]. In all of the models studied here, the amplitude of the seasonal cycle, as quantified by the difference in the maximum versus the minimum of the average seasonal cycle over different 39- or 40-year periods, increased between 1982-2020 and the 40-year period corresponding to the 2° warming level, and again for the period corresponding to the 3.2°C warming level.

Discussion & Conclusion

Our results show that maximum ocean temperatures – specifically annual maximum daily-mean sea surface temperatures – are excellently described by the generalised extreme value distribution over the past 39 years of global satellite observations. These results underscore the utility of the generalised extreme value distribution for investigating extreme ocean surface temperatures. Interestingly we find almost no evidence for heavier tails of maximum sea surface temperatures than that of the Gumbel distribution (i.e. almost no evidence that $\xi > 0$). A more positive ξ value is associated with a higher probability of 'extreme extremes' in SST. This is to some extent expected because there are numerous stabilising feedback processes for sea surface temperatures, including exchange with the atmosphere and both vertical and lateral mixing. It may also be because we analyze the observations at 1° resolution to facilitate comparison with models as spatial averaging necessarily truncates the tails of temperature maxima. It will be valuable in future work to further explore the dependency of GEV parameters to the spatial scale of analysis, particular with respect to ξ. That said, extreme temperature phenomena in the ocean occurring on larger scales (i.e. >1°) may be of greater interest due to their larger potential impacts, though the larger the spatial scale investigated, the less representative the average is of conditions experienced at a given location. We also find no evidence for non-stationarity in the detrended and deseasonalized SST anomalies, i.e. changes in the distribution of extremes over the historical period, though this may be due to small sample size and may be detectable in future work via large ensembles of historical simulations [8].

We have then used this theoretical distribution to compare observed and modelled annual maximum temperatures. While often-used definitions of marine heatwaves [20] differ from the simpler metric of maximum temperature, the two are very closely related [32]. Our analysis thus suggests that CMIP6 models capture both ocean maximum temperatures and marine heatwaves excellently on the whole. This comparison provides strong quantitative evidence that CMIP6 models are well-suited to making reliable projections about the future characteristics of marine heatwaves under continued climate change. While many studies have shown that the intensity and frequency of marine heatwaves will increase in the future [13, 31], our approach identifies regions where significant changes are expected for the ocean – i.e. where historical observations lie within the range of models' historical simulations and where this model range shifts significantly in the future. In agreement with previous studies [13, 31], our results indicate changes in the probability of extreme sea surface temperatures with global warming. In our analysis, the change in the location parameter dominates the shifts in the GEV distribution, corresponding to significant increases in annual SST maxima in the Indian Ocean, most of the Pacific Ocean, most of the Atlantic Ocean south of $\sim 40°$N, and portions of the Southern Ocean, for both scenarios and both warming levels considered here. This is consistent with previous analyses identifying trends in mean SST as the main driver of increases in marine heatwave frequency [13, 30]. Importantly, though maximum temperatures become significantly warmer over most of the ocean under a lower-emissions scenario, our results suggest that emissions reductions will substantially reduce the rate of increase in maximum temperatures, and likely therefore substantially reduce the harmful impacts of marine heatwaves on ocean ecosystems.

Materials and Methods

Observations

The observations we analyse are the 0.05° resolution, but regridded to 1°, satellite SST product from the European Space Agency (ESA) Climate Change Initiative (CCI) [27] (available via https://surftemp.net/, downloaded on June 10, 2022). It includes 39 complete years (1982-2020) and uses purely satellite-based observations without explicitly blending in-situ observations. This dataset is uniquely suited to our purposes because of its thorough validation and rigorous construction, and because it provides depth-adjusted SSTs de-aliased with respect to the diurnal cycle for direct comparison with model SSTs [27]. The data were regridded to 1° to facilitate comparison with the model realizations we were able to obtain (see below). Future work with higher resolution models should explore how GEV parameters depend on the spatial scale considered.

Model output

The model output we use is daily-mean SST (tos) output regridded to 1° resolution from the Earth system models that participated in the sixth phase of the Coupled Model Intercomparison Project (CMIP6, [10]). We were able to obtain one realisation of 14 different models, provided by 10 modelling centres (Table 1). We use the historical simulations over the 1850-2014 period and the future projections over 2015-2100 from the ScenarioMIP simulations [28], in particular the low emissions high mitigation scenario SSP1-2.6 and the high emission low mitigation scenario SSP5-8.5. We used the latter scenario simulations to determine the decades in which each model exceeds 2°C and 3.2°C of warming since preindustrial (i.e, 1850-1900) for Figure 3. 3.2°C was chosen because this was the maximum warming level possible to choose given the warming in the model realizations investigated here.

Statistical analysis

Different approaches exist to define MHWs [20, 19, 13, 32, 15]. Here we consider exclusively the annual maximum of daily-mean sea surface temperature (SST, unit of °C). We remove leap days from our analysis for simplicity. We only consider the latitudes 60°S-70°N because latitudes polewards of these are affected by sea ice, which strongly alters both the characteristics and measurement of sea surface temperature. For both observations and model output, we consider both the 'raw' maxima, i.e. the maximum daily-mean SST in a given year, and the maximum 'anomaly' from an interdecadal trend and a seasonal cycle. For the latter we regress SST against a 366-by-($365\times39=14{,}235$) matrix where the first row is 1, 2, 3... 14,235, and the remaining rows are given by horizontally repeating 365-by-365 identity matrices. This is equivalent to a linear trend model with a categorical variable for each day of the year. We then take the residuals from this regression for the anomalies. This allows us to simultaneously remove a linear interdecadal temperature trend and an annual seasonal cycle without making assumptions about the shape of the latter over the course of a year. Note however that this does assume a constant trend and seasonal cycle over time. Removing a seasonal cycle also means that maximum SST anomalies may occur at any point in the year, whereas maximum (raw) SSTs predominantly occur during times of year when average SSTs are already high.

We then fit these raw maxima and maximum anomalies by a generalized extreme value (GEV) distribution via maximum likelihood estimation using the 'mle' function in Matlab 2021b. The extreme value theorem states that the GEV distribution is the only possible limit distribution of properly normalized maxima of a sequence of independent and identically distributed (i.i.d.) random variables. Here we consider blocks of one year, i.e. annual maxima. Natural phenomena are rarely if ever truly i.i.d., but the GEV distribution holds and is applied broadly nonetheless [7], analogous to the central limit theorem holding quite accurately for only a handful of summed or multiplied random variables [3]. The GEV distribution has the form:

$$f(x;\mu,\sigma,\xi) = \frac{1}{\sigma}t(x)^{\xi+1}e^{-t(x)}$$

where $f(\cdot)$ is the probability density function and

$$t(x) = \begin{cases} (1+\xi(\frac{x-\mu}{\sigma}))^{-1/\xi} & \text{if } \xi \neq 0 \\ e^{-(x-\mu)/\sigma} & \text{if } \xi = 0 \end{cases}$$

so μ, and σ are the location, and scale parameters and ξ is the parameter that controls the shape of the distribution. A large positive ξ results in a heavy-tailed distribution while a negative value of ξ results in a light-tailed distribution. The extent to which the empirical distribution of maxima deviates from the GEV is then determined by calculating the Kuiper statistic V, which is the maximum of the hypothesized minus empirical cumulative distribution functions plus the maximum of the empirical minus hypothesized cumulative distribution function, i.e.

$$V = \max(E(x) - H(x)) + \max(T(x) - H(x))$$

where $E(x)$ is the empirical cumulative distribution function of x and $T(x)$ is the hypothesized empirical cumulative distribution function of x. This statistic is chosen over the more common Kolmogorov-Smirnov statistic $D = \max|E(x)-H(x)|$ because it gives equal weight to all portions of the distribution [12]. Repeating all analysis with D instead of V does not affect our conclusions. We first fit the GEV of the maximum anomalies, pooled across both all years and all locations; the parameters and V value associated with this fit are given in Figure 1. Given the excellent correspondence seen in Figure 1, we then fit the distribution of the 39 years of annual maximum temperatures (both raw and anomalies) at each location. The associated parameter values are given in Figure 2. In Figure 4, the standard (i.e. ± 1 standard deviation) uncertainties of the μ and σ values estimated for observations are shown;

these are calculated by the Wald method using the approximate Hessian matrix at the MLE estimates to compute standard errors. The same fitting procedure is then repeated both for globally pooled maximum anomalies and for local raw maxima and maximum anomalies for each model realisation, both for the historical period matching the observations and for future periods (see below).

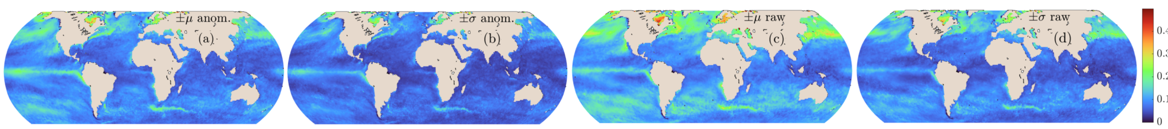

Figure 4: **Standard uncertainties of the maximum likelihood estimates for μ and σ in the satellite SST observations**.

Figure 3 shows the model ensemble mean of the parameter changes from 1982-2020 to a) 2061-2100 for SSP1-2.6, b) 2061-2100 for SSP5-8.5, c) the 40-year period centered around when 2° warming is reached in each model in in SSP5-8.5, and d) the 40-year period centered around when 3.2° warming is reached in each model in in SSP5-8.5. The black stippling indicates regions where the 90% range (i.e. the 5th-95th percentile) of the model ensemble distribution for each mapped quantity, estimated as the model ensemble mean plus or minus 1.645 times the model ensemble standard deviation (n.b. 1.645 is the z-score associated with the 95th percentile of a standard normal random variable), includes zero. The pink stippling indicates regions where the 90% range of the model ensemble distribution for each mapped quantity in the historical period does not include the observational estimate of that quantity. Figure 5 shows the same for σ in cases where the models agree in the sign of change over a nontrivial fraction of the ocean. In order to investigate whether these significant changes in Figure 5 were due to mean-SST trends or to changes in interannual variability, Figure 6 shows the ensemble-mean interannual SST variance, its change from 1982-2020 versus 2061-2100, and its change from 1982-2020 versus 2061-2100 after detrending. The absence of an increase in interannual variability in the latter case, and that we don't find scale changes for the detrended anomalies data, suggest that the apparent increase in σ is due to increasing warming trends over 2061-2100 in those regions, as in [13, 36].

In Table 1, in the global section, the V and parameter values are given for each model realisation by following the same procedure as in Figure 1 but for the historical model output rather than the observations. In the anomalies and raw sections, the r^2 values indicate the fraction of the variance explained in the observed parameters' (spatial) distribution by the models' parameters' (spatial) distributions. $r^2 = 1 - RSS/TSS$, where RSS is the residual sum of squares – here the residual being

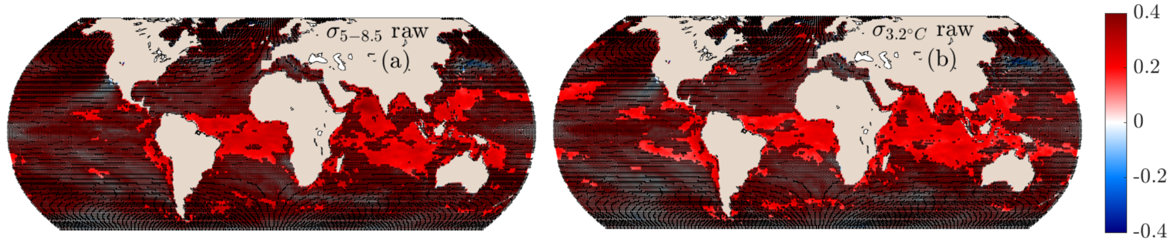

Figure 5: **CMIP6 ensemble mean change in σ parameter between the satellite period and 2061-2100 or after 3.2°C global warming**. As Figure 3 but for σ for SSP5-8.5 or the 3.2°C warming level.

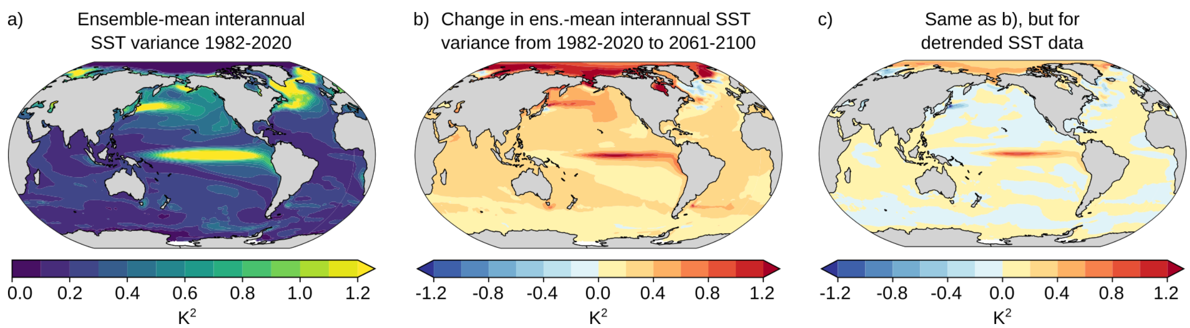

Figure 6: **CMIP6 ensemble mean interannual SST variance**. a) Ensemble-mean SST variance 1982-2020. b) Difference in ensemble-mean interannual SST variance 1982-2020 versus 2061-2100. c) same as (b) but when annual mean SSTs are (linearly) detrended.

the difference in a given parameter's values at each location for a given model versus the observations, and TSS is the total sum of squares for the observations. An $r^2 = 1$ thus indicates an everywhere perfect correspondence between the observed and modelled values. The $\tilde{V}$ values indicate the median value of V across GEV fits to all locations. For comparison we then generate 10,000 sets of 39 draws each from standard GEV(0,1,0) distribution and fit each of these with a GEV exactly like we do the sets of annual maximum temperatures. The median V value for these sets is 0.14, indicating we have effectively no evidence to reject the GEV on a local scale due to the sample size.

We tested for non-stationary by repeating the analysis shown in Figure 1 for the spatially pooled anomalies for individual years. Note that the raw SST data cannot be aggregated in space and fit with a GEV to test for non-stationarity in this way. We repeated this process both with globally pooled anomalies and with regionally pooled anomalies, defining regions corresponding to the equatorial and eastern tropical Pacific, the rest of the subtropics, and the subpolar regions poleward of 30N/S. None of the parameters exhibited a significant trend in any region (bootstrap 90% confidence intervals of trends, estimated by linear regression of parameter estimates versus year, all included zero), indicating a lack of strong non-stationarity in these data. Note that the anomalies include a linear interdecadal trend, but μ could be nonstationary even for these detrended data if maximum SST values were increasing significantly faster or slower than annual mean SSTs. This does not wholly exclude the possibility of non-stationarity of course, but given the small sample size of 39 years; a more thorough analysis of non-stationary behaviour is outside of the scope of this manuscript but may be fruitful to pursue in particular with large model ensembles with many realisations using a single model.

Acknowledgments: Cael led and Burger and Frölicher contributed substantially to all aspects of this work. Henson and Britten reviewed and edited the paper. The authors have no conflicts of interest to declare. Cael, Burger, Henson, and Frölicher acknowledge support from the European Union's Horizon 2020 Research and Innovation Programme under grant agreement No. 820989 (project COMFORT). Frölicher also acknowledges support from the European Union's Horizon 2020 Research and Innovation Programme under grant agreement No. 862923 (project AtlantECO) and the Swiss National Science Foundation (PP00P2-198897). GLB acknowledges funds from the Woods Hole Oceanographic Institution.The work reflects only the authors' view; the European Commission and their executive agency are not responsible for any use that may be made of the information the work contains.

References

[1] Michael A Alexander et al. "Projected sea surface temperatures over the 21st century: Changes in the mean, variability and extremes for large marine ecosystem regions of Northern Oceans". In: *Elementa: Science of the Anthropocene* 6 (2018).

[2] Gregory L Britten. "Extreme value distributions describe interannual variability in the seasonal North Atlantic phytoplankton bloom". In: *Limnology and Oceanography Letters* 7.3 (2022), pp. 269–276.

[3] BB Cael, Kelsey Bisson, and Christopher L Follett. "Can rates of ocean primary production and biological carbon export be related through their probability distributions?" In: *Global biogeochemical cycles* 32.6 (2018), pp. 954–970.

[4] Letıcia M Cavole et al. "Biological impacts of the 2013–2015 warm-water anomaly in the Northeast Pacific: winners, losers, and the future". In: *Oceanography* 29.2 (2016), pp. 273–285.

[5] William W L Cheung et al. "Marine high temperature extremes amplify the impacts of climate change on fish and fisheries". In: *Science Advances* 7.40 (2021), eabh0895. DOI: 10.1126/sciadv.abh0895.

[6] William W. L. Cheung and Thomas L. Frölicher. "Marine heatwaves exacerbate climate change impacts for fisheries in the northeast Pacific". In: *Scientific Reports* 10.1 (2020), p. 6678. DOI: 10.1038/s41598-020-63650-z.

[7] Anthony C Davison and Raphaël Huser. "Statistics of extremes". In: *Annual Review of Statistics and its Application* 2 (2015), pp. 203–235.

[8] Clara Deser et al. "Insights from Earth system model initial-condition large ensembles and future prospects". In: *Nature Climate Change* 10.4 (2020), pp. 277–286.

[9] Clara Deser et al. "Sea surface temperature variability: Patterns and mechanisms". In: *Annu. Rev. Mar. Sci* 2.1 (2010), pp. 115–143.

[10] Veronika Eyring et al. "Overview of the Coupled Model Intercomparison Project Phase 6 (CMIP6) experimental design and organization". In: *Geoscientific Model Development* 9.5 (2016), pp. 1937–1958.

[11] EM Fischer, Sebastian Sippel, and Reto Knutti. "Increasing probability of record-shattering climate extremes". In: *Nature Climate Change* 11.8 (2021), pp. 689–695.

[12] Brian P Flannery et al. "Numerical recipes in C". In: *Press Syndicate of the University of Cambridge, New York* 24.78 (1992), p. 36.

[13] Thomas L. Frölicher, Erich M. Fischer, and Nicolas Gruber. "Marine heatwaves under global warming". In: *Nature* 560.7718 (2018), pp. 360–364. DOI: 10.1038/s41586-018-0383-9.

[14] Melissa Gervais, Jeffrey Shaman, and Yochanan Kushnir. "Mechanisms Governing the Development of the North Atlantic Warming Hole in the CESM-LE Future Climate Simulations". In: *Journal of Climate* 31.15 (2018), pp. 5927–5946. DOI: 10.1175/JCLI-D-17-0635.1. URL: https://journals.ametsoc.org/view/journals/clim/31/15/jcli-d-17-0635.1.xml.

[15] Nicolas Gruber et al. "Biogeochemical extremes and compound events in the ocean". In: *Nature* 600.7889 (2021), pp. 395–407.

[16] Gaby Joanne Gründemann et al. "Rarest rainfall events will see the greatest relative increase in magnitude under future climate change". In: *Communications Earth & Environment* 3.1 (2022), pp. 1–9.

[17] F. Alexander Haumann, Nicolas Gruber, and Matthias Münnich. "Sea-Ice Induced Southern Ocean Subsurface Warming and Surface Cooling in a Warming Climate". In: *AGU Advances* 1.2 (2020), e2019AV000132. DOI: https://doi.org/10.1029/2019AV000132. URL: https://agupubs.onlinelibrary.wiley.com/doi/abs/10.1029/2019AV000132.

[18] Hakase Hayashida et al. "Insights into projected changes in marine heatwaves from a high-resolution ocean circulation model". In: *Nature communications* 11.1 (2020), pp. 1–9.

[19] Alistair J Hobday et al. "Categorizing and naming marine heatwaves". In: *Oceanography* 31.2 (2018), pp. 162–173.

[20] Alistair J. Hobday et al. "A hierarchical approach to defining marine heatwaves". In: *Progress in Oceanography* 141 (2016), pp. 227–238. DOI: https://doi.org/10.1016/j.pocean.2015.12.014.

[21] Neil J Holbrook et al. "A global assessment of marine heatwaves and their drivers". In: *Nature Communications* 10.1 (2019), pp. 1–13.

[22] Whitney K Huang et al. "Estimating changes in temperature extremes from millennial-scale climate simulations using generalized extreme value (GEV) distributions". In: *Advances in Statistical Climatology, Meteorology and Oceanography* 2.1 (2016), pp. 79–103.

[23] Terry P. Hughes et al. "Global warming and recurrent mass bleaching of corals". In: *Nature* 543.7645 (2017), pp. 373–377. ISSN: 0028-0836. DOI: 10.1038/nature21707.

[24] Charlotte Laufkötter, Jakob Zscheischler, and Thomas L. Frölicher. "High-impact marine heatwaves attributable to human-induced global warming". In: *Science* 369.6511 (2020), pp. 1621–1625. DOI: 10.1126/science.aba0690.

[25] Eun-Young Lee and Kyung-Ae Park. "Application of Non-stationary Extreme Value Analysis to Satellite-Observed Sea Surface Temperature Data for Past Decades". In: *Frontiers in Marine Science* (2022).

[26] Syukaro Manabe et al. "Transient responses of a coupled ocean–atmosphere model to gradual changes of atmospheric CO2. Part I. Annual mean response". In: *Journal of Climate* 4.8 (1991), pp. 785–818.

[27] Christopher J Merchant et al. "Satellite-based time-series of sea-surface temperature since 1981 for climate applications". In: *Scientific data* 6.1 (2019), pp. 1–18.

[28] Brian C O'Neill et al. "The scenario model intercomparison project (ScenarioMIP) for CMIP6". In: *Geoscientific Model Development* 9.9 (2016), pp. 3461–3482.

[29] Geert Jan van Oldenborgh et al. "Pathways and pitfalls in extreme event attribution". In: *Climatic Change* 166.1 (2021), pp. 1–27.

[30] Eric C. J. Oliver et al. "Longer and more frequent marine heatwaves over the past century". In: *Nature Communications* 9.1 (2018), p. 1324. DOI: 10.1038/s41467-018-03732-9.

[31] Eric C. J. Oliver et al. "Projected Marine Heatwaves in the 21st Century and the Potential for Ecological Impact". In: *Frontiers in Marine Science* 6 (2019), p. 734. DOI: 10.3389/fmars.2019.00734.

[32] Eric CJ Oliver et al. "Marine heatwaves". In: *Annual Review of Marine Science* 13 (2021), pp. 313–342.

[33] Dan A. Smale et al. "Marine heatwaves threaten global biodiversity and the provision of ecosystem services". In: *Nature Climate Change* 9.4 (2019), pp. 306–312. DOI: 10.1038/s41558-019-0412-1.

[34] Kathryn E. Smith et al. "Socioeconomic impacts of marine heatwaves: Global issues and opportunities". In: *Science* 374.6566 (2021), eabj3593. DOI: 10.1126/science.abj3593. URL: https://www.science.org/doi/abs/10.1126/science.abj3593.

[35] Huan Wang et al. "Frequency of the winter temperature extremes over Siberia dominated by the Atlantic Meridional Overturning Circulation". In: *npj Climate and Atmospheric Science* 5.1 (2022), pp. 1–10.

[36] T. Xu et al. "An increase in marine heatwaves without significant changes in surface ocean temperature variability". In: *Nature Communications* 13 (2022), p. 7396.